ARTICLE

CPSF4 regulates circRNA formation and microRNA mediated gene silencing in hepatocellular carcinoma

Xueying Wang[1] · Jiani Dong[1] · Xiaojing Li[2] · Zeneng Cheng[1] · Qubo Zhu [1]

Abstract

CircRNAs play essential roles in various physiological processes and involves in many diseases, in particular cancer. Global downregulation of circRNA expression has been observed in hepatocellular carcinoma (HCC) in many studies. Previous studies revealed that the pre-mRNA 3′ end processing complex participates in circRNA cyclization and plays an important role in HCC tumorigenesis. Therefore, we explored the role of CPSF4, for 3′ end formation and cleavage, in circRNA formation. Clinical research has shown that CPSF4 expression is upregulated in HCC and that high expression of CPSF4 is associated with poor prognosis in HCC patients. Mechanistic studies have demonstrated that CPSF4 reduces the levels of circRNAs, which possess a polyadenylation signal sequence and this decrease in circRNAs reduces the accumulation of miRNA and disrupts the miRNA-mediated gene silencing in HCC. Experiments in cell culture and xenograft mouse models showed that CPSF4 promotes the proliferation of HCC cells and enhances tumorigenicity. Moreover, CPSF4 antagonizes the tumor suppressor effect of its downstream circRNA in HCC. In summary, CPSF4 acts as an oncogene in HCC through circRNA inhibition and disruption of miRNA-mediated gene silencing.

Introduction

Hepatocellular carcinoma (HCC) is the most common primary liver malignancy and the fourth leading cause of cancer-related mortality worldwide. The slow development of HCC involves the accumulation of genetic mutations and dysregulated gene expression over time [1–4]. Since noncoding RNAs (ncRNAs) play important roles in epigenetic regulation of gene expression at the transcriptional and posttranscriptional levels, numerous ncRNAs are involved in the tumorigenesis and metastasis of HCC [4, 5]. Circular RNAs (circRNAs) are a type of single-stranded endogenous RNA that forms a covalently closed continuous loop structure [6]. As an evolutionarily conserved ncRNA across phyla, circRNAs play essential roles in various physiological processes [7, 8], such as binding with miRNAs as competitive endogenous RNAs (ceRNAs) [9, 10], regulating gene transcription in RNA-protein complexes [10], and even encoding proteins [11]. Many types of human diseases are associated with circRNAs; in particular cancer, circRNAs have been reported to be involved in tumorigenesis, metastasis, and drug resistance [12]. Moreover, because circRNAs lack the 5′ cap and 3′ poly (A) tail and therefore are rarely degraded by exonuclease RNase, circRNAs are expected to be more stable tumor markers and better therapeutic targets than other RNAs [13].

Interestingly, the ratio of a circRNA to its linear counterpart is always lower in tumors than in normal samples and even lower in immortal cancer cell lines and this ratio negatively correlates with the proliferation index of cancer cells [14]. Many circRNAs have been reported to be reduced in HCC and inhibit the development of HCC, such as hsa_circ_0018665 [15], hsa_circ_0000847 [16], and hsa_circ_0007874 [17]. A previous explanation for the global reduction in circRNA expression was that circRNAs are passively dispersed by cell proliferation. However, we hypothesized that circRNA formation might be inhibited and that the expression of circRNAs is actively reduced in HCC cells.

✉ Qubo Zhu
  qubozhu@csu.edu.cn

1   Xiangya School of Pharmaceutical Sciences in Central South University, Changsha, China

2   Shanghai General Hospital, Shanghai, China

Although the back-splicing of circRNAs is different from the canonical splicing of linear RNAs, the two processes share the same splicing and maturation factors, including various snRNAs and protein components [18]. Therefore, the cis- and trans-elements that regulate pre-mRNA alternative splicing (AS) and alternative polyadenylation (APA) can also affect RNA circularization [19]. Recent genome-wide protein-RNA interaction studies demonstrated that AS and APA are two closely related processes and that 3′ end formation factors play an important role in AS, including cleavage and polyadenylation specificity factor (CPSF), cleavage stimulation factor (CSTF), cleavage factor Im (CFIm), and cleavage factor IIm (CFIIm) [20, 21]. Among them, CPSF is the core component of the 3′ end processing complex that specifically recognizes the polyadenylation signal sequence (PAS: AAUAAA or its variants including: AUUAAA, AAUAUA, AAUGAA, AAUAAU, and AAGAAA) and catalyzes cleavage [22]; CSTF specifically recognizes the U/GU-rich elements, and is required for cleavage [23]; CFIm binds with two UGUA sequences, and facilitates the assembly of the 3′ end processing complex [3]; CFIIm takes part in the polyadenylation process [24]. In our previous studies, we found that NUDT21, an important subunit of CFIm, promotes circRNA cyclization; and its low expression in HCC reduces the circRNA level [2, 3, 25]. Therefore, we aimed to determine whether CPSF, as the core performer of PAS site cleavage, is also abnormally expressed in HCC and thereby regulates circRNA formation.

CPSF is a multisubunit complex consisting of CPSF1, CPSF2, CPSF3, CPSF4 FIP1L1, and WDR33 [20]. Among these subunits, CPSF1, CPSF4, Fip1, and WDR33 form a stable tetramer complex that localizes CPSF to the PAS site [26], and recent genome-wide crosslinking immunoprecipitation (CLIP) studies revealed that only WDR33 and CPSF4 bind to the AAUAAA sequence directly [22]. Through analysis of the cancer genome atlas (TCGA) database, we found that the expression of CPSF1, CPSF3, and CPSF4 was significantly upregulated in HCC, and the survival analysis also showed that the overall survival (OS) rate of patients with high CPSF2 CPSF3, and CPSF4 expression patients were significantly shortened. In addition, previous studies revealed that CPSF4 is highly expressed in colon cancer [27], breast cancer [28], and lung cancer [29] and is closely related to the tumorigenesis and metastasis of these tumors. Since CPSF4 expression is significantly increased in HCC, and its high level corresponds to a high risk for poor patient survival, we focused our research on the correlation between CPSF4 and HCC.

MicroRNAs (miRNAs) posttranscriptionally silence gene expression by base-pairing with partially complementary sequences in the 3′ untranslated regions (UTRs) of target mRNAs [30]. Since circRNAs can function as sponges to bind with miRNAs [31], downregulation of circRNA expression disrupts miRNA-mediated gene silencing. In fact, general downregulation of miRNA expression is observed in tumors compared with normal tissues in multiple cancers, including HCC [32]. In-depth research revealed that only circRNAs with perfect complementarity to their target miRNAs could degenerate miRNAs directly through AGO2-mediated degradation, most circRNAs are only partially complementary to their target miRNAs and instead serve as miRNA storage pools to prevent their degradation by RNA exonuclease cleavage. Thus, destabilization of circRNA expression through acute intervention (e.g., with siRNAs, shRNAs, or ASOs) usually results in increased miRNA release and repression of the corresponding targets. In a different scenario, the prolonged absence of a sponge circRNA, due to chronic treatments, led to the degradation of its binding miRNAs and an increase in the expression of the corresponding targets [33]. The global decrease in miRNA levels in tumors reported previously [32] is most likely caused by the overall decline in circRNAs in tumor cells.

In summary, a global decrease in circRNAs, an increase in CPSF4, and general downregulation in miRNA are three obvious features that occur simultaneously in HCC, and these features appear to be tightly associated with each other. Therefore, we hypothesized that the increase in CPSF4 enhances the recognition of PAS signals and the cleavage of circRNAs, which leads to a global decrease in circRNAs in HCC. Due to the prolonged absence of sponge circRNA storage pools, miRNAs are no longer protected and are degraded, enabling oncogenes to evade miRNA regulation and, thus, induce HCC tumorigenesis and metastasis.

Results

CircRNAs were globally down-regulated in HCC tissues

To explore the circRNA profiles in HCC, several publicly available data were analyzed, including GSE94508 [34], GSE97332 [17], and GSE14520 [35]. The volcano plot and box plot both showed that circRNA levels were globally dropped in HCC in all 3 GEO databases (Supplementary Fig. 1A, B). Although widespread RNA shortening by alternative cleavage and polyadenylation is a common phenomenon in cancer [36], the length distribution of circRNAs was not changed, and all the circRNAs' levels were dropped regardless of their length (Supplementary Fig. 1C). Analysis of the PAS sequence, which is the core element for polyadenylation cleavage, showed that circRNAs with or without PAS sequences

were both down-regulated significantly in HCC tissues. However, the average levels of the PAS-contained circRNAs were significantly lower than the PAS free circRNAs in all three GEO databases (Supplementary Fig. 1D), which indicated that PAS mediated cleavage played an important role in circRNA formation. In summary, circRNAs were globally decreased in HCC tissues, and PAS mediated RNA cleavage might be one of the reasons that led to the down-regulation of circRNA in HCC.

High CPSF4 expression was associated with poor prognosis in HCC patients

Since CPSF is the core performer for PAS cleavage, we hypothesized that the abnormality of CPSF would influent circRNA biogenesis and result in the tumorigenesis of HCC. From the mRNA sequence data in the TCGA database, 3 out of the 6 CPSF components were identified to be significantly over-expressed in HCC, which were CPSF1, CPSF3, and CPSF4; and the fold changes were 1.8 ± 0.7, 1.5 ± 0.4, and 1.8 ± 0.8, respectively (Supplementary Fig. 2A). The analysis of the associations between the CPSF proteins and the OS of patients demonstrated that the OS of CPSF2, CPSF3, and CPSF4 high expression patients was significantly shorter than the low expression patients; and the HRs were 1.6, 1.7, and 1.8, respectively (Supplementary Fig. 2B).
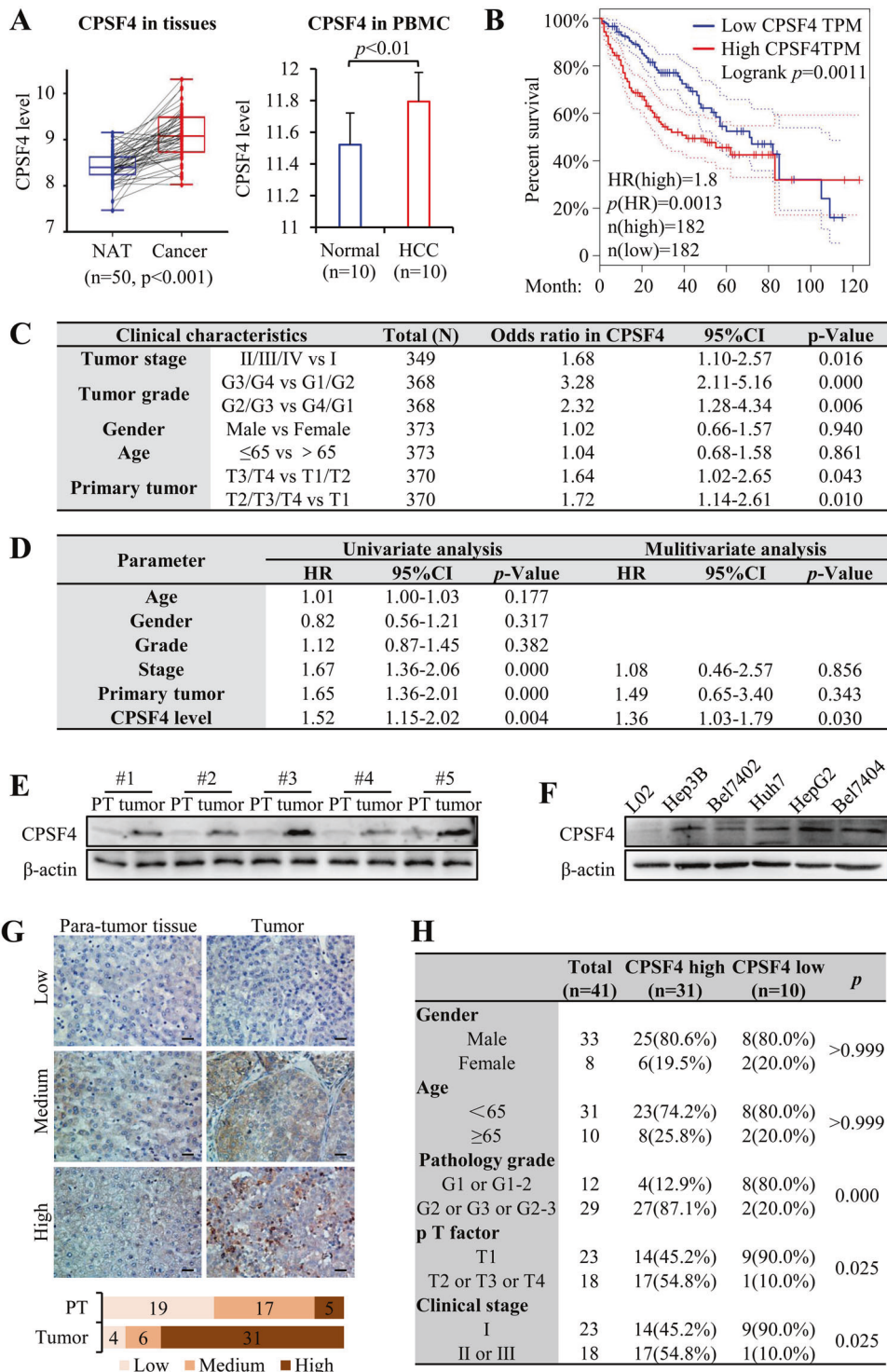
Since CPSF4 expression is significantly increased in HCC, and its high level corresponds to the highest risk for OS in HCC, we focused our research on CPSF4. By comparing the sequence data of 50 matched pairs, we found that CPSF4 mRNA levels were significantly higher in HCC tissues compared with those in normal adjacent tissues (NATs). The microarray data from GSE49515 also demonstrated that the CPSF4 levels in peripheral blood mononuclear cell (PBMC) samples from 10 HCC patients were significantly higher compared to 10 controlled healthy individuals, which suggested that CPSF4 was a suitable biomarker for HCC diagnosis (Fig. 1A). Kaplan–Meier survival analysis of 364 patients also showed that the 5-year survival rate was dropped from $57\% \pm 5\%$ in CPSF4 low expression patients to $42\% \pm 5\%$ in CPSF4 high expression patients, and the HR between these two groups was 1.8 ($p < 0.01$, Fig. 1B). Further correlation analysis illustrated that CPSF4 was significantly correlated with clinical TNM stage, pathology grade, and clinical stage (Fig. 1C). The univariate analysis indicated an association between the OS rates of HCC patients and high CPSF4 expression ($p < 0.01$); and the multivariate Cox regression analysis revealed that the CPSF4 level (HR $= 1.36$; $p = 0.03$) was an independent prognostic factor for OS (Fig. 1D).

The bioinformatic results were further validated by analysis of clinical specimens. In the tested five cases, the western blot of CPSF4 displayed higher expression in HCC compared to their PT tissues (Fig. 1E). In addition, the protein level of CPSF4 in cell lines also showed that CPSF4 was highly expressed in all HCC cell lines (Hep3B, Bel7402, Huh7, HepG2, and Bel7404), but could be barely detected in the normal liver cell L02 (Fig. 1F). Among the five HCC cell lines, HepG2 had the highest level, while Bel7402 had the lowest level of CPSF4. We constructed CPSF4 knockdown and overexpression cells in both Bel7402 and HepG2 cells (Supplementary Fig. 3). But since CPSF4 in Bel7402 is very low, we cannot detect the significant knockdown efficiency in Bel7402-KD cells; while CPSF4 in HepG2 is very high, the overexpression efficiency is also very low in HepG2-OE cells. Thus, in later researches, most of the CPSF4 KD experiments were done in HepG2 cells, while most of the CPSF4 OE experiments were done in Bel7402 cells. Immunohistochemistry (IHC) staining of human HCC tissue microarrays, composed of 41 pairs of tissue samples, also confirmed the up-regulation of CPSF4 in HCC tissues (Supplementary Table 1). Among the 41 cases, 25 HCC tissues showed strong CPSF4 expression. In the contrast, most of the PT tissues showed weak or medium CPSF4 expression (Fig. 1G). The correlation analysis also illustrated that CPSF4 expression was significantly correlated with the clinical TNM stage, pathology grade, and clinical stage (Fig. 1H).

CPSF4 reduced the level of circRNAs in HCC cells

Since CPSF4 is responsible for the PAS cleavage, we hypothesized that the increase of CPSF4 accelerated the cleavage of circRNAs and reduced their level in HCC cells. To test this hypothesis, total RNAs from CPSF4-KD HepG2 cells, CPSF4-OE Bel7402 cells, and their negative controls were extracted and analyzed by high-throughput sequencing (Supplementary Tables 2 and 3). Sequence data showed that more down-regulated circRNAs (1058) than up-regulated circRNAs (821) were detected in CPSF4-OE cells, and the average level of circRNA was significantly decreased. In contrast, most of the circRNAs (3221 out of 5005 circRNAs) in CPSF4-KD cells were up-regulated, and the average level of circRNA was significantly increased (Figs. 2A, B). Through bioinformatics analysis showed that CPSF4 mainly inhibited exonic circRNAs, but a small portion of inhibited circRNAs were intronic or intronic-exonic circRNAs. Length distribution of circRNAs was altered in neither the CPSF4-OE cells nor the CPSF4-KD cells (Fig. 2C), but the circRNA alternations after CPSF4 modulation were PAS dependent on. First, the expressions of PAS-contained circRNAs were significantly lower than PAS-free circRNAs in all 4 cell lines. Second, obvious up-regulation tendency was detected after CPSF4 KD in circRNAs with PAS sequence; but no changes were detected in circRNAs without PAS sequence (Fig. 2D). To our surprise, the circRNAs with or without the PAS sequence were both decreased after CPSF4 OE; maybe some

A CPSF4 in tissues   CPSF4 in PBMC

B

C

Clinical characteristics		Total (N)	Odds ratio in CPSF4	95%CI	p-Value
Tumor stage	II/III/IV vs I	349	1.68	1.10-2.57	0.016
Tumor grade	G3/G4 vs G1/G2	368	3.28	2.11-5.16	0.000
	G2/G3 vs G4/G1	368	2.32	1.28-4.34	0.006
Gender	Male vs Female	373	1.02	0.66-1.57	0.940
Age	≤65 vs > 65	373	1.04	0.68-1.58	0.861
Primary tumor	T3/T4 vs T1/T2	370	1.64	1.02-2.65	0.043
	T2/T3/T4 vs T1	370	1.72	1.14-2.61	0.010

D

Parameter	Univariate analysis			Mulitivariate analysis		
	HR	95%CI	p-Value	HR	95%CI	p-Value
Age	1.01	1.00-1.03	0.177			
Gender	0.82	0.56-1.21	0.317			
Grade	1.12	0.87-1.45	0.382			
Stage	1.67	1.36-2.06	0.000	1.08	0.46-2.57	0.856
Primary tumor	1.65	1.36-2.01	0.000	1.49	0.65-3.40	0.343
CPSF4 level	1.52	1.15-2.02	0.004	1.36	1.03-1.79	0.030

E   **F**

G Para-tumor tissue   Tumor   **H**

	Total (n=41)	CPSF4 high (n=31)	CPSF4 low (n=10)	p
Gender				
Male	33	25(80.6%)	8(80.0%)	>0.999
Female	8	6(19.5%)	2(20.0%)	
Age				
<65	31	23(74.2%)	8(80.0%)	>0.999
≥65	10	8(25.8%)	2(20.0%)	
Pathology grade				
G1 or G1-2	12	4(12.9%)	8(80.0%)	0.000
G2 or G3 or G2-3	29	27(87.1%)	2(20.0%)	
p T factor				
T1	23	14(45.2%)	9(90.0%)	0.025
T2 or T3 or T4	18	17(54.8%)	1(10.0%)	
Clinical stage				
I	23	14(45.2%)	9(90.0%)	0.025
II or III	18	17(54.8%)	1(10.0%)	

non-specific PAS sequences other than the six traditional PAS sequences could also be cleaved in the presence of a high level of CPSF4.

To validate the sequence data, we first selected 807 down-regulated circRNAs (fold change > 2, $p < 0.05$) in HCC tissues from the GEO database; then, we screened 1447 circRNAs that were either down-regulated in CPSF4-OE cells or up-regulated in CPSF4-KD cells from RNA-seq data. Data in the intersection of these two sets, which contained 24 circRNAs, were the candidate circRNAs for validation; and

◀ **Fig. 1 CPSF4 is highly expressed in HCC tissues and higher expression of CPSF4 indicates a poor prognosis for HCC patients. A** The TCGA database analysis shows significantly higher expression of CPSF4 mRNA in HCC tissues than in NATs ($n = 50$, $p < 0.001$). Analysis of the GSE49515 dataset microarray data shows that CPSF4 levels in PBMC samples from HCC patients are significantly higher than in samples from healthy individuals ($n = 10$, $p < 0.01$). Error bars indicate standard deviation. **B** Kaplan–Meier analysis of the OS rate for HCC patients with different expression levels of CPSF4 with a log-rank test shows that the OS rate is significantly worse in patients with a high expression of CPSF4. **C** The association between CPSF4 and patient clinicopathological features was analyzed by logistic regression analysis. The CPSF4 level was significantly correlated with the clinical TNM stage, pathology grade, and clinical stage. **D** Univariate analysis and multivariate analysis of the clinical parameters were performed using the Cox regression model, which revealed that the CPSF4 level ($HR = 1.36$; $p = 0.03$) was an independent prognostic factor for the OS rate. **E** The expression of CPSF4 in HCC tissues and their corresponding NATs from five different patients was measured by western blot. β-actin was used as the internal control. **F** The expression of CPSF4 in five HCC cell lines and a normal liver cell line was measured detected by western blot. β-actin was used as the internal control. **G** The tissue microarray shows CPSF4 expression in HCC tissues and their NATs observed by immunohistochemical staining. The upper panel lists the representative images and the bottom panel is the statistical analysis. **H** Association of CPSF4 expression with patient clinicopathological features was analyzed by χ2 test, which revealed that higher expression of CPSF4 indicates a poor prognosis.

the structure analysis showed 16 of them contained PAS elements. Real-time PCR results showed that 13 out of these 16 circRNAs were suppressed in CPSF4 OE cells, but activated in CPSF4 KD cells (Fig. 2E). Two circRNAs with PAS element, hsa_circ_0027774, and hsa_circ_0004913, were chosen as the typical CPSF4 targeted circRNAs; while, another widely studied circRNA without PAS element, hsa_circ_0001946, was selected as CPSF4 non-targeted circRNA. Northern blot results demonstrated that hsa_circ_0027774 and hsa_circ_0004913 were negatively correlated with CPSF4, but hsa_circ_0001946 kept the same level in all cell lines (Fig. 2F). The OE plasmids of these three circRNAs were also constructed and co-transfected with CPSF4 OE or KD plasmids, and the real-time PCR results showed that circRNAs with PAS (hsa_circ_0027774 and hsa_circ_0004913) were negatively correlated with CPSF4 level while circRNA without PAS (hsa_circ_0001946) was not affected by the CPSF4 (Fig. 2G), which illuminated that CPSF4 suppressed circRNA post-transcriptionally. In summary, CPSF4 directly regulated the expression of circRNA with PAS elements in HCC cells.

PAS element was critical for the cyclization of circRNA

To clarify the importance of PAS sequences in circRNA biogenesis, we used the previously constructed IRES-derived pCircGFP reporter as the parent plasmid and generated a mutated GFP-reporter plasmid with an AAUAAA element

inserted in front of IRES (Fig. 3A). From confocal microscopy, we found that the GFP fluorescence intensity of mutated GFP-reporter was obviously decreased compared to the parent plasmid (Fig. 3B), which suggested that PAS elements were critical for the circRNA cyclization. To check the involvement of CPSF4 in circRNA biogenesis, the mutated GFP-reporter was co-transfected with or without the Cy3-linked siCPSF4, and confocal microscopy showed that the fluorescence intensity in the siCPSF4 transfected cells was much stronger than the siRNA non-transfected cells (Fig. 3C). Real-time PCR and western blot also showed that GFP expression of mutated GFP-reporter was lower than that of parent GFP-reporter; and siCPSF4 treatment could increase both the circRNA and protein levels of GFP in the mutated GFP-reporter transfected cells but not the parent GFP-reporter transfected cells (Fig. 3D, E). All these data demonstrated that CPSF4 regulated circRNA biogenesis through the interaction with the PAS element.

CPSF4 mediated circRNA decreasing reduced the accumulation of miRNA and disrupted the miRNA mediated gene silencing

To test whether CPSF4 mediated circRNA decreasing would affect the miRNA stability, total small RNAs from CPSF4-OE and CPSF-KD cells were extracted and analyzed with Agilent 2100 Bioanalyzer. The size distribution of small RNA showed that the ratio between the miRNA (4 nt to 40 nt) and tRNA (40 nt to 80 nt) decreased in CPSF4-OE cells, but increased in CPSF4-KD cells (Fig. 4A–C), which confirmed that CPSF4 abolished the accumulation of miRNA.

Just like other cancers, the miRNA levels are globally decreased in HCC (Supplementary Fig. 4A–C). Interestingly, most of the down-regulated miRNAs were partially complementary to the 807 down-regulated circRNAs we screened before. We picked hsa-miR-383-5p and hsa-miR-142-5p, which were partially complementary to hsa_circ_0004913; and hsa-miR-450b-3p and hsa-miR-145-5p, which were partially complementary to hsa_circ_0027774; for further analysis (Supplementary fig. 4D). Real-time PCR showed that all the four miRNAs were increased in CPSF4-KD cells, and decreased in CPSF4-OE cells (Fig. 4D). CircRNA probe precipitation in HepG2 cells confirmed that hsa-miR-145 and hsa-miR-450b bound with hsa_circ_0027774, while hsa-miR-142 and hsa-miR-383 bound with hsa_circ_0004913. AGO2 immunoprecipitation (RIP) assay also showed that hsa_circ_0004913, hsa_circ_0027774, and their binding miRNAs were specifically enriched in AGO2 antibody-associated complex, but not in the control IgG. In CPSF4-KD cells, the hsa_circ_0004913/has-miR-383, and the hsa_circ_0027774/hsa-miR-145 RNA pairs were increased compared to the control cells; but in CPSF4-OE cells, these two pairs of binding RNA were
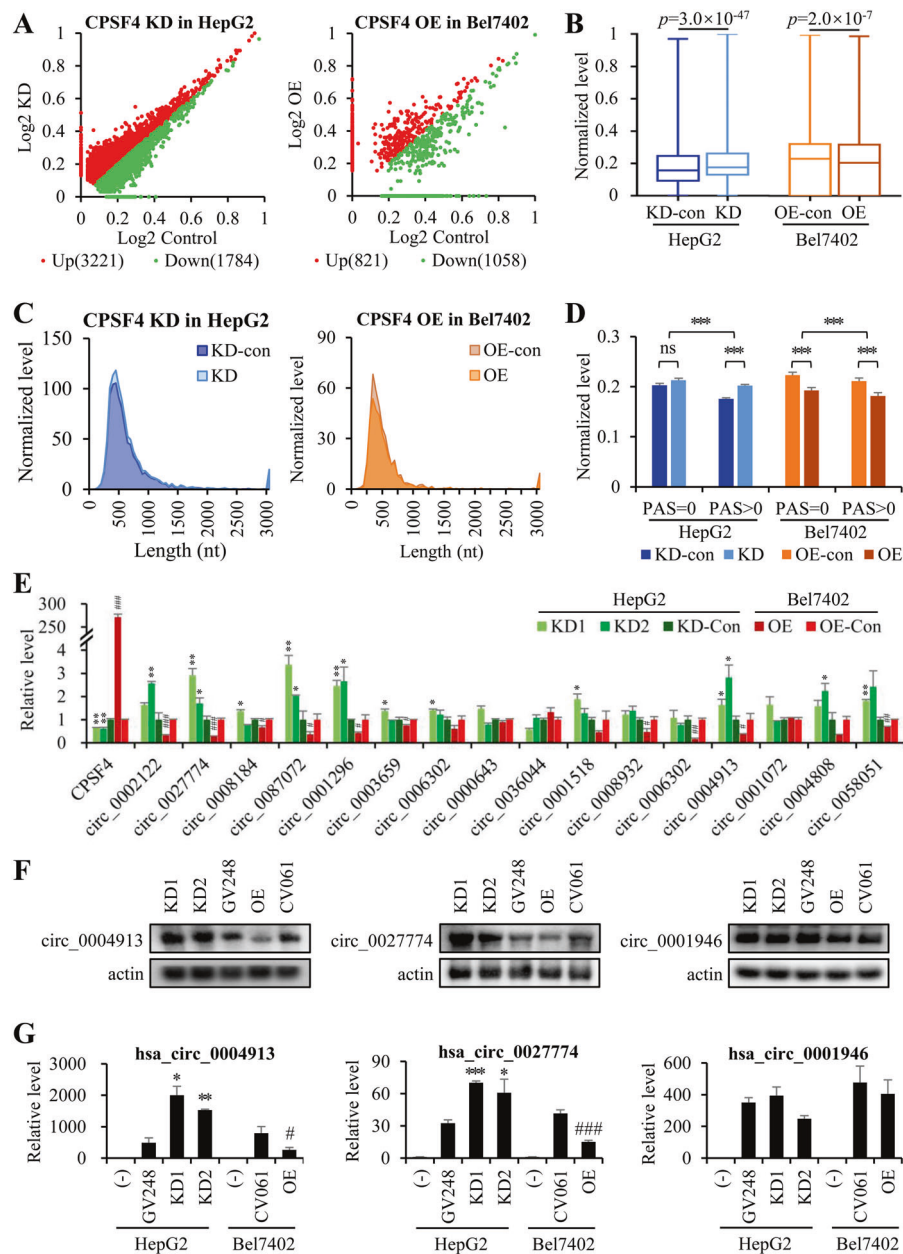
Fig. 2 CPSF4 reduces the circRNA biogenesis in HCC cells. A–D Statistical analysis of high-throughput sequencing data. **A** There were more circRNAs with downregulated expression circRNAs with upregulated expression in CPSF4-OE cells, while the opposite was true for CPSF4-KD cells. The X-axis represents the Log_2 level of circRNAs in control cells, while the Y-axis represents the Log_2 level of circRNAs in CPSF4 KD or OE cells. CircRNAs with downregulated expression are marked in green, and those with upregulated expression are marked in red. **B** The box plot shows that the overall circRNA level is significantly increased in CPSF4-KD cells, but decreased in CPSF4-OE cells. **C** The length distribution patterns of circRNAs were similar between these two sets of cell lines. **D** The gene expression profile reveals that the circRNA alterations after CPSF4 modulation are PAS sequence-dependent since circRNAs with PAS elements are affected after CPSF4 variation, while circRNAs without PAS elements are not affected after CPSF4 KD. Error bars indicate standard error mean. **E** The expression of 16 circRNAs, which were downregulated in the GSE database and significantly altered after CPSF4 modulation based on sequencing data, was measured by real-time PCR in CPSF4-KD and CPSF4-OE cell lines generated in HepG2 and Bel7402 cells, respectively. **F** The circRNA levels in CPSF4-KD and CPSF4-OE cells were measured by Northern blot; the β-actin probe was used as the internal control. **G** The circRNA OE plasmids were cotransfected with CPSF4-KD or CPSF4-OE plasmids, and exogenous circRNAs were measured by real-time PCR. In (**E**)–(**G**), KD1 and KD2 indicate knockdown plasmids/cells, and the KD plasmids/cells were compared to the GV248 vector: $*p < 0.05$, $**p < 0.01$, $***p < 0.001$. OE indicates overexpression plasmids/cells and the OE plasmids/cells were compared to the CV061 vector: $\#p < 0.05$, $\#\#p < 0.01$, $\#\#\#p < 0.001$. Error bars indicate standard deviation ($n = 3$).

Fig. 3 The PAS sequence is critical for CPSF4-mediated RNA cyclization. A Schematic diagram of the pCircGFP reporter structure, inserted AAUAAA sequences are marked. **B** A laser scanning confocal microscope documents the distribution and fluorescence intensity of circ-GFP (green) for both parent (upper panels) and mutated (lower panels) circ-GFP plasmids in HepG2 cells. The nuclei were counterstained with DAPI (blue). **C** CPSF4-silencing promotes the biogenesis of circ-GFP expressing AAUAAA sequences since the GFP fluorescence intensity is higher in siCPSF4 cells (above) than in the control group (below). The CPSF4 siRNA is labeled by cy5 dyestuff [44]. In (**B**) and (**C**), scale bar = 10 µM. **D** The mRNA levels of both the parent and mutated circ-GFP were measured by real-time PCR, and β-actin was used as the internal control. Error bars indicate standard deviation ($n = 3$). **E** The GFP protein levels of parent and mutated circ-GFP were measured by western blot, β-actin was used as the internal control.
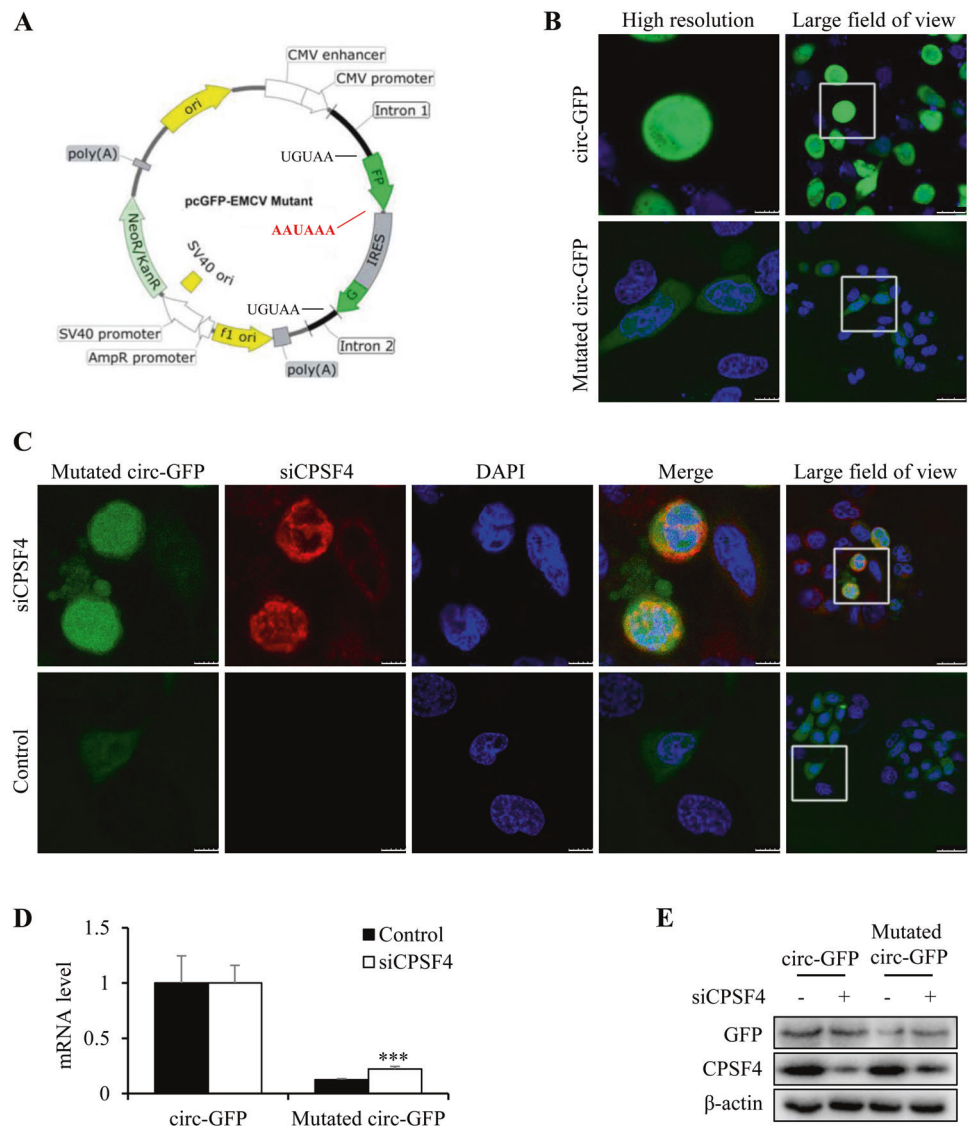
decreased compared to the control cells, which suggested that CPSF4 mediated circRNA decreasing reduced the miRNAs accumulation (Supplementary Fig. 5A, B). MiR-383 was identified to directly target PARP2 in HCC [37], and PARP2 was involved in the tumor development of HCC [37, 38]. MiR-145 directly targeted CDCA3 [39], and CDCA3 reduced the survival time of HCC patients [40]. Luciferase assay confirmed that miR-145 could silence CDCA3 expression and miR-383 could silence PARP2 expression (Supplementary fig. 5C). Bioinformatics analysis also showed there were 2 miR-383 binding sites in the 3′-UTR of PARP2 and 2 miR-145 binding sites in the 3′-UTR of CDCA3 (Supplementary Fig. 6A). Moreover, these 2 genes were both overexpressed in HCC, and their high expression was correlated with shorter OS in HCC patients (Supplementary Fig. 6B, C). The protein levels of PARP2 and CDCA3 detected by western blot also illustrated that

both PARP2 and CDCA3 were decreased in CPSF4 KD cells, and increased in CPSF4 OE cells (Fig. 4E). In addition, the expressions of these two proteins were positively correlated with CPSF4 expression in HCC (Supplementary Fig. 6D). All these data confirmed that CPSF4 mediated circRNA decreasing disrupted the miRNA mediated gene silencing.

CPSF4 promoted the proliferation of HCC cells and enhanced the tumorigenicity in xenografts mice models

To characterize the effect of CPSF4 on HCC progression, the growth rate and clonogenicity of both CPSF4-KD and CPSF4-OE cells were monitored. MTT assay demonstrated that silencing of CPSF4 inhibited the cell growth; while overexpression of CPSF4 promoted the cell growth (Fig.
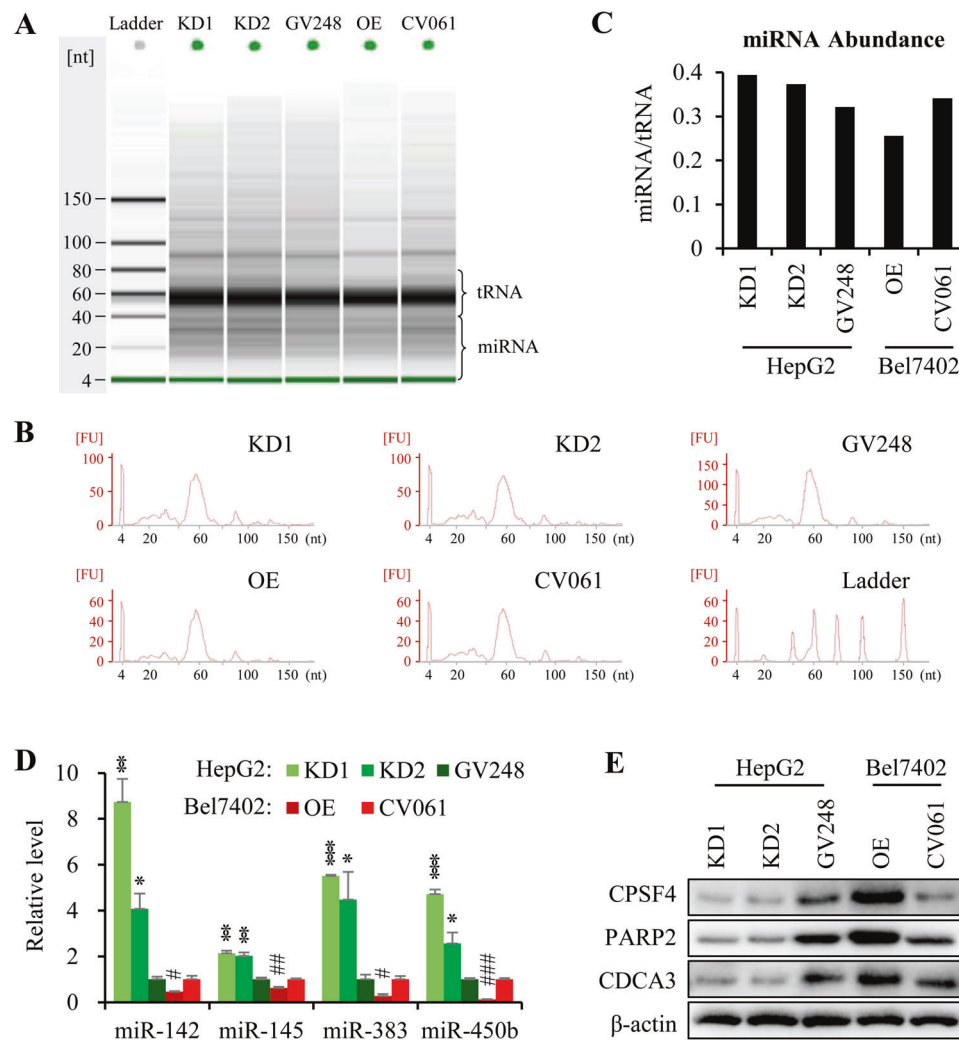
Fig. 4 CPSF4 reduced the accumulation of miRNA and gene silencing. [45] Small RNA analysis performed by using the Agilent 2100 Bioanalyzer indicates that CPSF4 abolishes the accumulation of miRNA since the ratio between the miRNA and tRNA decreases in CPSF4-OE cells, but increases in CPSF4-KD cells. **A** shows the electronic gel image of small RNA. **B** Shows the size distribution of small RNA. The *X*-axis represents the RNA length, and the *Y*-axis represents the RNA intensity. **C** The ratio between the miRNA and tRNA was calculated for each sample. **D–E** The effects of CPSF4 on miRNAs and their target genes were confirmed in two circRNA-miRNA-mRNA pathways: hsa_circ_0004913/hsa_miR_383-5p/PARP2 and hsa_circ_0027774/hsa_miR_145-5p/CDCA3. **D** The miRNA levels were measured by real-time PCR, and β-actin was used as the internal control. KD1 and KD2 cells were compared to GV248 vector-transfected control HepG2 cells: $*p < 0.05$, $**p < 0.01$, $***p < 0.001$. OE cells were compared to CV061 vector-transfected control Bel7402 cells: $\#p < 0.05$, $\#\#p < 0.01$, $\#\#\#p < 0.001$. Error bars indicate standard deviation ($n = 3$). **E** The protein levels of miRNA target genes in stable cell lines were measured by western blot. CPSF4 levels were also measured, and β-actin was used as the internal control.

5A). Soft agar assays also showed that CPSF4-KD cells generated less and smaller colonies; while CPSF4-OE cells generated more and larger colonies (Fig. 5B, C). Next, in xenograft mice model, KD of CPSF4 significantly inhibited tumor growth, and the weights of CPSF4-KD cell derived xenograft tumor were significantly lower than the control tumors after 20 days growth (Fig. 5D–G). Moreover, both real-time PCR and immunohistochemistry analysis of the tumor tissues exhibited that long time suppression of CPSF4 induced the expression of hsa_circ_0004913, hsa_circ_0027774, and their binding miRNAs (hsa-miR-145 and hsa-miR-383); but repressed the expression of PARP2 and CDCA3 (Fig. 5H, I). All these results confirmed that CPSF4 disrupted circRNA/miRNA pathways and played an important role in HCC tumorigenesis.

CPSF4 antagonized the tumor suppression effect of hsa_circ_0004913

Hsa_circ_0004913 had been reported to be a potential tumor suppressor for HCC [41]. To test whether CPSF4 promoted tumorigenesis of HCC through hsa_circ_0004913 inhibition,

Fig. 5 CPSF4 promotes the proliferation and tumorigenicity of HCC cells.
A MTT assays show that OE of CPSF4 increases cell growth, while KD of CPSF4 represses the growth in both Bel7402 and HepG2 cells. Error bars indicate standard deviations ($n = 5$).
**B–C** Colony formation assays in Bel7402 and HepG2 cells demonstrate that CPSF4-KD cells generate fewer and smaller colonies than GV248 control cells, while CPSF4-OE cells generate more and larger colonies than CV061 control cells. **B** Is the statistical analysis. Error bars indicate standard deviations ($n = 3$). Comparison with GV248 control cells, $*p < 0.05$, $**p < 0.01$, $***p < 0.001$. Comparison with CV061 control cells: $\#p < 0.05$, $\#\#p < 0.01$, $\#\#\#p < 0.001$. **C** shows the representative graphs. **D** Images of tumor size 21 days after transplantation of HepG2 cells. **E** The tumors were photographed after removal from nude mice ($n = 8$). **F** Tumor diameters were measured at a regular interval of 2 days for up to 20 days and the tumor volumes were calculated. Error bars indicate the standard deviation ($n = 8$). **G** The tumors were weighed after removal from nude mice ($n = 8$). **H** The expression levels of circRNAs and their binding miRNAs were measured by real-time PCR. Error bars indicate the standard deviation ($n = 3$). **I** Immunohistochemistry staining shows the expression of CPSF4, CDCA3, and PARP2 in tumor tissues. Hematoxylin and eosin staining show histopathology. Scale bar, 20 μm.
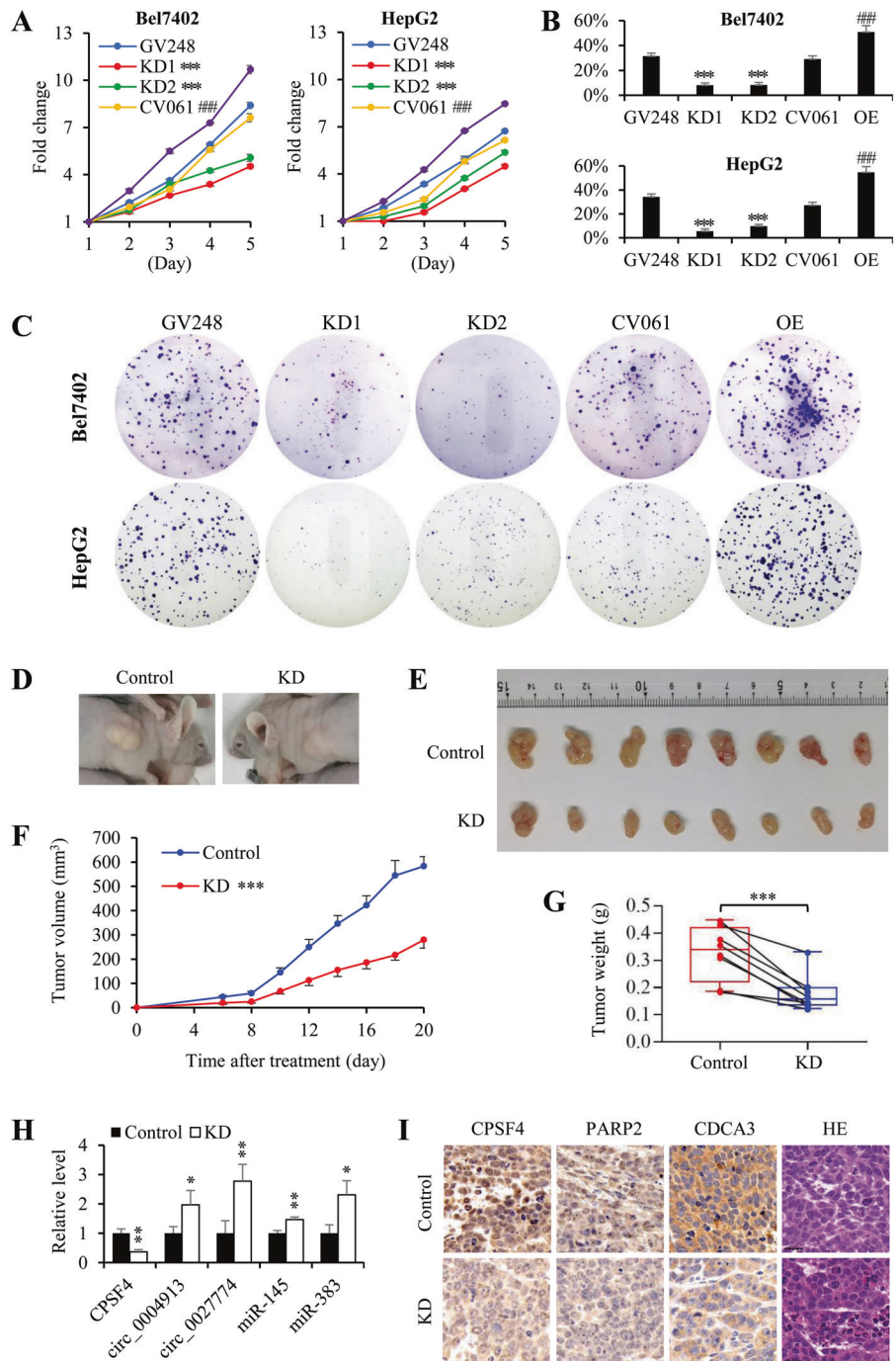

we generated hsa_circ_0004913 OE cells in both Bel7402 and HepG2 cells, and then transfected them with CPSF4 plasmid. The CPSF4 proteins and the hsa_circ_0004913 level in each cell line were detected by western blotting and real-time PCR, respectively (Fig. 6A, B). As predicted, hsa_circ_0004913-OE cells showed slower proliferation and lower clonogenicity compared to the control cells. However, OE of CPSF4 could abrogate the tumor suppression effects of hsa_circ_0004913, as the growth rate and clone formation ability recovered after CPSF4 transfection (Fig. 6C, D).

These results indicated the important role for circRNA in CPSF4-mediated tumorigenesis of HCC cells.

Discussion

Owing to the continuous progress in circRNA identification methodologies, the understanding of circRNAs has dramatically changed over the past several years, from rare transcriptional byproducts, to evolutionarily conserved

Fig. 6 CPSF4 antagonizes the tumor suppression effect of hsa_circ_0004913. A, B The confirmation of the establishment of the hsa_circ_0004913 OE stable cell line and hsa_circ_0004913/ CPSF4 double OE stable cell line. **A** Hsa_circ_0004913 levels were measured by real-time PCR. Error bars indicate standard deviation ($n = 3$). **B** CPSF4 levels were measured by western blots. **C** MTT assays show that OE of hsa_circ_0007874 represses cell growth, and the growth rate recovered after CPSF4 transfection in both Bel7402 and HepG2 cells. Comparison with empty control cells, $*p < 0.05$, $**p < 0.01$, $***p < 0.001$. Comparison with hsa_circ_0004913 OE cells, $\#p < 0.05$, $\#\#p < 0.01$, $\#\#\#p < 0.001$. Error bars indicate standard deviations ($n = 5$). **D** Colony formation assays demonstrate that hsa_circ_0004913-OE cells show lower clonogenicity than the control cells, and OE of CPSF4 abrogates the repression effect of hsa_circ_0004913. The left panels show the representative graphs, and the right panels show the statistical analysis. Error bars indicate standard deviations ($n = 3$).
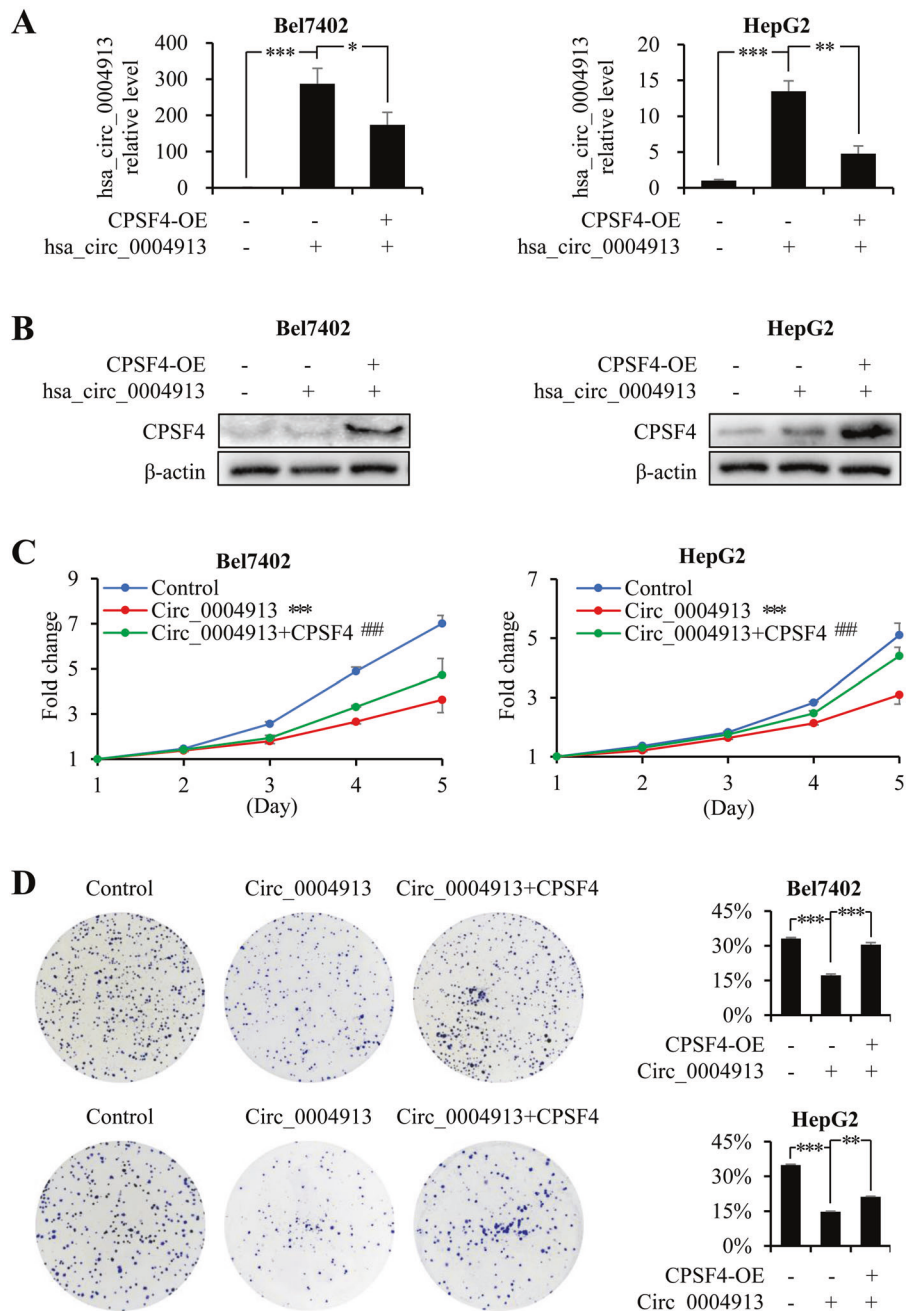
molecules that participate in diverse physiological processes [42]. Over the past few years, numerous circRNAs have been shown to participate in the tumorigenesis, metastasis, and drug resistance of HCC; and have been suggested as therapeutic targets or biomarkers for the diagnosis and prognosis of HCC [43]. Biological function studies have shown that many circRNAs contribute to HCC progression by modulating the proliferation, invasion, metastasis, and apoptosis of HCC cells by interacting with miRNAs [43]. However, why, and how these circRNAs are abnormally expressed in HCC has not yet been fully elucidated. Previous studies showed that back-splicing of circRNA and canonical splicing of linear RNA shared the same splicing and maturation factors[19], and RNA cleavage factors involved in AS and APA also participate in circRNA biogenesis [2, 19]. Therefore, as the core component for RNA 3′ end cleavage, the CPSF complex likely participates in the biogenesis of circRNA.

From clinical specimens and bioinformatics analysis, we found that circRNA expression was globally downregulated in HCC tissues, while CPSF4 expression was upregulated, and the high expression of CPSF4 was associated with poor prognosis of HCC patients. High-throughput sequencing data demonstrated that overexpression of CPSF4 decreased

the overall circRNA level, whereas knockdown of CPSF4 increased the overall circRNA level. Moreover, the circRNAs with PAS elements were influenced by the CPSF4 expression level more substantially than the PAS-free circRNAs. These sequencing data were further confirmed by Real-time PCR and Northern blot, since CPSF4 could modulate the levels of circRNA whit PAS elements but had little impact on circRNA without PAS elements. The importance of the PAS sequence in RNA cyclization was also validated using a GFP-reporter plasmid containing the AAUAAA sequence. Cell culture and xenograft mouse model experiments demonstrated that CPSF4 promotes the proliferation of HCC cells and enhances tumorigenicity. In-depth studies showed that CPSF4 antagonized the tumor suppression effect of hsa_circ_0004913, which suggested that the oncogenic role of CPSF4 in HCC is at least partially realized through circRNA inhibition.

CPSF4 functions as an oncogene in many cancers, including colon cancer, breast cancer, and lung cancer. Previous studies have focused on the roles of CPSF4 in the hTERT pathway and COX-2/NF-κB pathway [27–29]. Based on our research, a new theory is proposed for the mechanism of CPSF4 in HCC as follows: upregulation of CPSF4 expression in HCC cells inhibits the formation of circRNA; in the prolonged absence of sponge circRNAs, miRNAs are degraded, and the expression of their corresponding target genes increases by evading miRNA-mediated gene silencing, which finally results in uncontrolled cell proliferation (Fig. 7). The activation of the hTERT and COX-2 genes by CPSF4 reported previously may occur not only through transcriptional activation, but also through the circRNA/miRNA pathway.

Material and methods

Bioinformatic analysis

CircRNA expression data were downloaded from the gene expression omnibus (GEO) database (https://www.ncbi.nlm.nih.gov/geo/), and the data were converted into logarithmic form (Supplementary Tables 4–6). To compare the three sets of data in parallel, all data were normalized to a 0–1 scale in later analysis. Gene and miRNA expression data were retrieved from TCGA database (https://portal.gdc.cancer.gov/) or GEO database. The Kaplan–Meier survival curve and the box plot of TCGA-LIHC patients were generated on the GAPIA (http://gepia.cancer-pku.cn/). For pathway analysis, the circRNA/miRNA interaction was predicted by CircInteractome (http://circinteractome.nia.nih.gov/), CircAtlas (http://circatlas.biols.ac.cn/) and CircFunBase (http://bis.zju.edu.cn/CircFunBase/); the miRNA/mRNA interaction was predicted by TargetScan (http://www.targetscan.
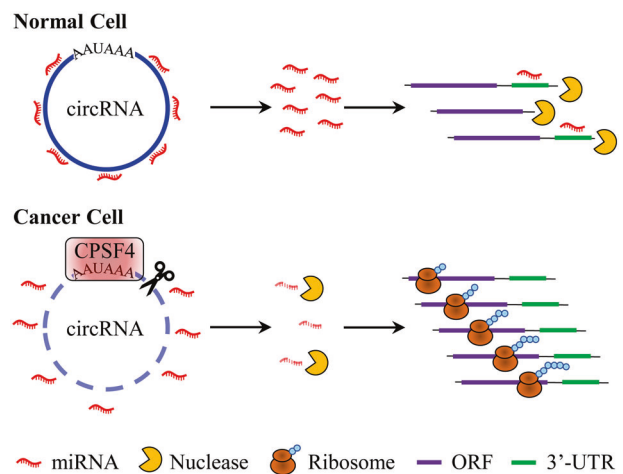

Fig. 7 Schematic diagram of how CPSF4 regulates circRNA biogenesis in HCC. The increased expression of CPSF4 in HCC cells enhances the recognition of the PAS in circRNA and the cleavage of circRNA by the CPSF complex, thereby reducing the expression of circRNA. CircRNAs act as miRNA sponges, and the reduction of their expression will increase miRNA degradation by nuclease. Some oncogenes in cancer cells escape the regulation of miRNAs and are overexpressed, eventually leading to uncontrolled tumor proliferation. The upper panel represents normal cells with low CPSF4 expression. The lower panel represents the cancer cells with high CPSF4 expression. ORF: open reading frame.

org/); and the co-expression correlation was analyzed by Cbioportal (http://www.cbioportal.org/).

Clinical cancer samples and tissue microarrays

Five cancer samples were obtained from the Third Xiangya Hospital of Central South University and stored in liquid nitrogen. The study was approved by the Ethics Committee of the Third Xiangya Hospital of Central South University, and all experiments were conducted in accordance with the Declaration of Helsinki and good clinical practice guidelines (Supplementary file 1).

The tissue microarrays of HCC were obtained from Shanghai Outdo Biotech Co., Ltd. (Shanghai, China). All tissue samples were obtained from the patients without anti-cancer treatment before tumor resection. Information from all patients was available in Supplementary Table 1.

Cells culture and plasmid transfection

HepG2 (RRID:CVCL_0027), Bel7402 (RRID:CVCL_549), Hep3B (RRID:CVCL_0326), Bel7404 (RRID:CVCL_6568), Huh-7(RRID:CVCL_0336), and L02 (RRID:CVCL_6926) cells were purchased from the Xiangya Experiment Center (Changsha, China), and were authenticated and tested for mycoplasma contamination before use. The cell culture was performed as described in REF [2].

CPSF4 shRNAs were inserted into a GV248 vector to generate CPSF4-knockdown (KD) plasmids. The CPSF4 mRNA sequence (NM_001318161) was inserted into a CV061 vector to construct a CPSF4-overexpressing (OE) plasmid. Hsa_circ_0004913, hsa_circ_0027774, and hsa_circ_0001946 OE plasmids were constructed by Geneseed Biotech Co., Ltd. (Guangzhou, China) in pCD25-ciR vector. The CPSF4 siRNA/shRNA sequences were provided in Supplementary Table 7. All the plasmids or siRNA were transfected into cells via viaFect™ Transfection reagent (Promega, Madison, WI) or siRNA transfection reagents (GenePharma, Shanghai, China).

RNA quality control and sequencing

The RNA samples were extracted using TRIzol reagent (Invitrogen, Carlsbad, CA), and analyzed with Agilent 2100 Bioanalyzer (Agilent, Santa Clara, CA). Qualified RNA samples were sent to Biomarker Technologies (Beijing, China) for sequencing, and the final sequencing was conducted by the TruSeq SR Cluster Kit v3-cBot-HS (Illumina) and the Illumina hiseq Xten sequencer.

Molecular biology experiments

The RT-PCR, real-time PCR, Northern blot assay, Western blot assay, and luciferase reporter assay were performed as described in REF [2]. The primers, probes, and miRNA mimics were provided in Supplementary Table 7. The antibodies used in Western blot assay were anti-CPSF4 (1:1000, DF12260, Affinity, RRID: AB_2845065), anti-PARP2 (1:1000, 55149-1-AP, Proteintech, RRID: AB_10858796), anti-CDCA3 (1:1000, 15594-1-AP, Proteintech, RRID: AB_2878154) or anti-β-actin (1:3000, ab8227, Abcam, RRID: AB_722539).

AGO2 RIP assay

RNA-IP was performed using the Protein A/G magnetic beads (Bimake, Houston, TX), and immunoprecipitation was performed using the control IgG (#3900, CST) and anti-Ago2 antibody (ab57113, Abcam). The RNA complexes were isolated through phenol-chloroform extraction and analyzed via qPCR assays.

circRNA probe precipitation

Biotin-labeled probes were synthesized by Tsingke Biotechnology (Beijing, China)(Supplementary Table 7). The HepG2 cells were fixed using 4% formaldehyde for 15 min, lysed, sonicated, and centrifuged. Then the supernatant was incubated with circRNA probes and Dynabeads M-280 Streptavidin (Thermo Scientific) overnight at 30 °C. The next day, the mixture was washed and lyzed in 200 μL of lysis buffer and proteinase K. Finally, the RNA mixture was extracted using Trizol and detected by qPCR.

Cell growth rate assay and clonogenicity assay

The specific protocols were described previously in REF [2]. The MTT assay was repeated five times and the colony formation assay was repeated three times for each cell line.

Xenograft tumorigenic assays

HepG2 cells ($2–4 \times 10^6$) were subcutaneously injected into the lateral backside of eight male BALB/c nude mice (5 weeks old). CPSF4-KD cells were implanted into the left side, while control cells were implanted into the right side of each mouse. The tumor size was measured by calipers every two days. After 3 weeks of growth, the mice were euthanized, and the xenografts were harvested and weighed. Group assignment and tumor monitoring were carried out double-blinded. Then, the tumors were fixed in neutral buffered formalin, and embedded in paraffin. Hematoxylin and eosin (H&E) staining and immunohistochemical analysis were performed for histopathological evaluations of the tissues.

Power analysis was performed with G*Power online analysis freeware, using repeated-measures ANOVA with between-subjects factors. Animal welfare and experimental procedures were carried out in accordance with the Guide for the Care and Use of Laboratory Animals (Ministry of Science and Technology of China, 2006) and approved by the animal ethics committee of Central South University (Supplementary file 1).

Statistical analysis

R software package (R Version 3.5.2), SPSS16.0, and GraphPad Prism 5 software packages were performed for statistical analysis. Statistical significance was determined by the Student t-test or ANOVA followed by a post hoc Bonferroni test. Logistic regression model and Cox analysis were used to estimate the association between CPSF4 and clinical risks.

All p values were two-sided, and differences with $p < 0.05$ were considered statistically significant (*$p < 0.05$, **$p < 0.01$, ***$p < 0.001$). All statistical experimental data were presented as mean ± sd.

Compliance with ethical standards

Conflict of interest The authors declare no competing interests.

Publisher's note Springer Nature remains neutral with regard to jurisdictional claims in published maps and institutional affiliations.

References

1. Yang JD, Hainaut P, Gores GJ, Amadou A, Plymoth A, Roberts LR. A global view of hepatocellular carcinoma: trends, risk, prevention and management. Nat Rev Gastroenterol Hepatol. 2019;16:589–604.
2. Li X, Ding J, Wang X, Cheng Z, Zhu Q. NUDT21 regulates circRNA cyclization and ceRNA crosstalk in hepatocellular carcinoma. Oncogene. 2020;39:891–904.
3. Sun M, Ding J, Li D, Yang G, Cheng Z, Zhu Q. NUDT21 regulates 3′-UTR length and microRNA-mediated gene silencing in hepatocellular carcinoma. Cancer Lett. 2017;410:158–68.
4. Zhang H, Sheng C, Yin Y, Wen S, Yang G, Cheng Z, et al. PABPC1 interacts with AGO2 and is responsible for the microRNA mediated gene silencing in high grade hepatocellular carcinoma. Cancer Lett. 2015;367:49–57.
5. Wang Z, Li X. The role of noncoding RNA in hepatocellular carcinoma. Gland Surg. 2013;2:25–29.
6. Greene J, Baird AM, Brady L, Lim M, Gray SG, McDermott R, et al. Circular RNAs: biogenesis, function and role in human diseases. Front Mol Biosci. 2017;4:38.
7. Ding J, Zhou W, Li X, Sun M, Ding J, Zhu Q. Tandem DNAzyme for double digestion: a new tool for circRNA suppression. Biol Chem. 2019;400:247–53.
8. Qu S, Zhong Y, Shang R, Zhang X, Song W, Kjems J, et al. The emerging landscape of circular RNA in life processes. RNA Biol. 2017;14:992–9.
9. Hansen TB, Jensen TI, Clausen BH, Bramsen JB, Finsen B, Damgaard CK, et al. Natural RNA circles function as efficient microRNA sponges. Nature. 2013;495:384–8.
10. Wilusz JE, Sharp PA. Molecular biology. A circuitous route to noncoding RNA. Science. 2013;340:440–1.
11. Meng X, Chen Q, Zhang P, Chen M. CircPro: an integrated tool for the identification of circRNAs with protein-coding potential. Bioinformatics. 2017;33:3314–6.
12. Xu S, Zhou L, Ponnusamy M, Zhang L, Dong Y, Zhang Y, et al. A comprehensive review of circRNA: from purification and identification to disease marker potential. PeerJ. 2018;6:e5503.
13. Enuka Y, Lauriola M, Feldman ME, Sas-Chen A, Ulitsky I, Yarden Y. Circular RNAs are long-lived and display only minimal early alterations in response to a growth factor. Nucleic Acids Res. 2016;44:1370–83.
14. Bachmayr-Heyda A, Reiner AT, Auer K, Sukhbaatar N, Aust S, Bachleitner-Hofmann T, et al. Correlation of circular RNA abundance with proliferation-exemplified with colorectal and ovarian cancer, idiopathic lung fibrosis, and normal human tissues. Sci Rep. 2015;5:8057.
15. Song C, Li D, Liu H, Sun H, Liu Z, Zhang L, et al. The competing endogenous circular RNA ADAMTS14 suppressed hepatocellular carcinoma progression through regulating microRNA-572/regulator of calcineurin 1. J Cell Physiol. 2019;234:2460–70.
16. Zhang X, Luo P, Jing W, Zhou H, Liang C, Tu J. circSMAD2 inhibits the epithelial-mesenchymal transition by targeting miR-629 in hepatocellular carcinoma. Onco Targets Ther. 2018;11:2853–63.
17. Han D, Li J, Wang H, Su X, Hou J, Gu Y, et al. Circular RNA circMTO1 acts as the sponge of microRNA-9 to suppress hepatocellular carcinoma progression. Hepatology. 2017;66:1151–64.
18. Qu S, Yang X, Li X, Wang J, Gao Y, Shang R, et al. Circular RNA: a new star of noncoding RNAs. Cancer Lett. 2015;365:141–8.
19. Liang D, Tatomer DC, Luo Z, Wu H, Yang L, Chen LL, et al. The output of protein-coding genes shifts to circular RNAs when the pre-mRNA processing machinery is limiting. Mol Cell. 2017;68:940–54. e943
20. Misra A, Green MR. From polyadenylation to splicing: dual role for mRNA 3′ end formation factors. RNA Biol. 2016;13:259–64.
21. Misra A, Ou J, Zhu LJ, Green MR. Global promotion of alternative internal exon usage by mRNA 3′ end formation factors. Mol Cell. 2015;58:819–31.
22. Chan SL, Huppertz I, Yao C, Weng L, Moresco JJ, Yates JR 3rd, et al. CPSF30 and Wdr33 directly bind to AAUAAA in mammalian mRNA 3′ processing. Genes Dev. 2014;28:2370–80.
23. Takagaki Y, Manley JL. RNA recognition by the human polyadenylation factor CstF. Mol Cell Biol. 1997;17:3907–14.
24. Noble CG, Beuth B, Taylor IA. Structure of a nucleotide-bound Clp1-Pcf11 polyadenylation factor. Nucleic Acids Res. 2007;35:87–99.
25. Tan S, Li H, Zhang W, Shao Y, Liu Y, Guan H, et al. NUDT21 negatively regulates PSMB2 and CXXC5 by alternative polyadenylation and contributes to hepatocellular carcinoma suppression. Oncogene. 2018;37:4887–900.
26. Clerici M, Faini M, Aebersold R, Jinek M. Structural insights into the assembly and polyA signal recognition mechanism of the human CPSF complex. Elife 2017;6:e33111.
27. Yang Q, Fan W, Zheng Z, Lin S, Liu C, Wang R, et al. Cleavage and polyadenylation specific factor 4 promotes colon cancer progression by transcriptionally activating hTERT. Biochim Biophys Acta Mol Cell Res. 2019;1866:1533–43.
28. Wu J, Miao J, Ding Y, Zhang Y, Huang X, Zhou X, et al. MiR-4458 inhibits breast cancer cell growth, migration, and invasiveness by targeting CPSF4. Biochem Cell Biol. 2019;97:722–30.
29. Yi C, Wang Y, Zhang C, Xuan Y, Zhao S, Liu T, et al. Cleavage and polyadenylation specific factor 4 targets NF-kappaB/cyclooxygenase-2 signaling to promote lung cancer growth and progression. Cancer Lett. 2016;381:1–13.
30. Fabian MR, Sonenberg N. The mechanics of miRNA-mediated gene silencing: a look under the hood of miRISC. Nat Struct Mol Biol. 2012;19:586–93.
31. Zhong Y, Du Y, Yang X, Mo Y, Fan C, Xiong F, et al. Circular RNAs function as ceRNAs to regulate and control human cancer progression. Mol Cancer. 2018;17:79.
32. Lu J, Getz G, Miska EA, Alvarez-Saavedra E, Lamb J, Peck D, et al. MicroRNA expression profiles classify human cancers. Nature. 2005;435:834–8.
33. Bezzi M, Guarnerio J, Pandolfi PP. A circular twist on microRNA regulation. Cell Res. 2017;27:1401–2.
34. Fu L, Yao T, Chen Q, Mo X, Hu Y, Guo J. Screening differential circular RNA expression profiles reveals hsa_circ_0004018 is associated with hepatocellular carcinoma. Oncotarget. 2017;8:58405–16.
35. Yu J, Xu QG, Wang ZG, Yang Y, Zhang L, Ma JZ, et al. Circular RNA cSMARCA5 inhibits growth and metastasis in hepatocellular carcinoma. J Hepatol. 2018;68:1214–27.
36. Mayr C, Bartel DP. Widespread shortening of 3′UTRs by alternative cleavage and polyadenylation activates oncogenes in cancer cells. Cell. 2009;138:673–84.

37. Zhou Q, Zhang W, Wang ZF, Liu SY. Long non-coding RNA PTTG3P functions as an oncogene by sponging miR-383 and up-regulating CCND1 and PARP2 in hepatocellular carcinoma. BMC Cancer. 2019;19:1–11.

38. Canhui Y, Wang Y, Zhang C, et al. Cleavage and poly-adenylation specific factor 4 targets NF-κB/cyclooxygenase-2 signaling to promote lung cancer growth and progression. Cancer Lett. 2016;381:1–13.

39. Chen Q, Zhou L, Ye X, Tao M, Wu J. miR-145-5p suppresses proliferation, metastasis and EMT of colorectal cancer by targeting CDCA3. Pathol Res Pract. 2020;216:152872.

40. Wu BW, Huang Y, Luo YW, Ma A, Wu ZX, Gan YC, et al. The diagnostic and prognostic value of cell division cycle associated gene family in hepatocellular carcinoma. J Cancer. 2020;11:5727–37.

41. Lin X, Chen Y. Identification of potentially functional CircRNA-miRNA-mRNA regulatory network in hepatocellular carcinoma by integrated microarray analysis. Med Sci Monit Basic Res. 2018;24:70–78.

42. Ebermann C, Schnarr T, Muller S Recent advances in under-standing circular RNAs. F1000Res. 2020;9:F1000 Faculty Rev-655.

43. Qiu L, Xu H, Ji M, Shang D, Lu Z, Wu Y, et al. Circular RNAs in hepatocellular carcinoma: Biomarkers, functions and mechanisms. Life Sci. 2019;231:116660.

44. Trifonov A, Sharon E, Tel-Vered R, Kahn JS, Willner I. Application of the hybridization chain reaction on electrodes for the amplified and parallel electrochemical analysis of DNA. J Phys Chem C. 2016;120:15743–52.

45. Chang C-C, Chen C-Y, Chuang T-L, Wu T-H, Wei S-C, Liao H, et al. Aptamer-based colorimetric detection of proteins using a branched DNA cascade amplification strategy and unmodified gold nanoparticles. Biosens Bioelectron. 2016;78:200–5.